Acta Cryst. (1997). B**53**, 870–879

Electron Density Distribution in LiB_3O_5 at 293 K

C. Le Hénaff,[a] N. K. Hansen,[a] J. Protas[a]* and G. Marnier[b]

[a]*Laboratoire de Cristallographie et Modélisation des Matériaux Minéraux et Biologiques, Unité Associée au CNRS 809, Université Henri-Poincaré, Nancy I, BP 239, F-54506 Vandoeuvre-lès-Nancy CEDEX, France, and* [b]*Laboratoire de Physique, Equipe Matériaux pour l'Optique, Unité Associée au CNRS 1796, Université de Bourgogne, Faculté des Sciences Mirande, BP 138, 21004 Dijon CEDEX, France. E-mail: protas@lcm3b.u-nancy.fr*

(*Received 6 January 1997; accepted 23 May 1997*)

Abstract

The electron density distribution in lithium triborate LiB_3O_5 has been studied at room temperature by X-ray diffraction using Ag $K\alpha$ radiation up to 1.02 $Å^{-1}$ [1439 unique reflections with $I > 3\sigma(I)$]. Conventional refinements with a free-atom model yield $R(F) = 0.0223$, $wR(F) = 0.0299$, $S = 1.632$. Atom charge refinements show that the lithium should be considered a monovalent ion. Multipolar refinements were undertaken up to fourth order, imposing local non-crystallographic symmetry constraints in order to avoid phase problems leading to meaningless multipole populations due to the non-centrosymmetry of the structure (space group: $Pna2_1$). The residual indices decreased to: $R(F) = 0.0147$, $wR(F) = 0.0193$, $S = 1.106$. The net charges are in good agreement with what can be expected in borate chemistry. Deformation density maps are analysed in terms of σ and π bonding. The experimental electron distribution in the p_z orbitals of triangular B atoms and surrounding O atoms has been analysed by introducing idealized hybridized states. In parallel, the electron density has been determined from *ab initio* Hartree–Fock calculations on fragments of the structure. Agreement with the X-ray determination is very good and confirms the nature of bonding in the crystal. The amount of transfer of π electrons from the oxygen to the triangular B atoms is estimated to be 0.22 electrons by theory.

1. Introduction

A number of studies have already been devoted to electron density distribution or to electrostatic properties calculations in borates by X-ray diffraction during the last decade: $LiBO_2$ (Kirfel, Will & Stewart, 1983), orthoboric acid $B(OH)_3$ (Gajhede, Larsen & Rettrup, 1986; Sommer-Larsen, Kadziola & Gajhede, 1990), calcium metaborate $Ca(BO_2)_2$ (Kirfel, 1987), lithium tetraborate LiB_4O_7 (Radaev, Muradyan, Malakhova, Burak & Simonov, 1989), lithium triborate LiB_3O_5 (Radaev, Genkina, Lomonov, Maximov, Pisarevskii, Chelokov & Simonov, 1991; Radaev, Maximov, Simonov, Andreev & D'yakov, 1992). LiB_3O_5 is of special interest due to its non-linear optical properties, particularly for second harmonic generation of UV light (Chen, Wu, Jiang, Wu, You, Li & Lin, 1989). The two studies recently published by Radaev *et al.* (1991, 1992) describe qualitatively the electron density distribution in LiB_3O_5, but do not include any modelling of the valence-electron density. The aim of this study is to improve the bonding model derived from experimental evidence (Le Hénaff, 1996). Theoretical maps of the valence-electron density are also given and compared with the experimental ones.

2. Experimental

Table 1 summarizes crystal data and data collection conditions. The high melting point of ~ 1107 K (Sastry & Hummel, 1958; Chen *et al.*, 1989) is favourable to preclude the need for performing the measurements at low temperatures. The crystal was grown by a flux method (Marnier, 1986, 1988; Marnier, Boulanger & Ménaert, 1989). The single crystal used was extracted mechanically from the solid growth bath.

The lattice parameters are in good agreement with those of Radaev *et al.* (1991, 1992).

Three high-angle reflections at $\theta > 23°$ were used to control the crystal orientation every 100 reflections, possibly followed by an automatic recentring.

The profile analysis was carried out using Blessing's (1987, 1988) program package, which also corrects for Lorentz and polarization effects and variations of the intensities of the standard reflections. Taking into account the low value of the absorption factor [$\mu(LiB_3O_5$, Ag $K\alpha$) = 1.272 cm^{-1}] and the small crystal size (mean radius $r = 0.015$ cm), the absorption correction is very low and does not vary within the θ Bragg range. No absorption correction was made. 5388 reflections having $I > 3\sigma(I)$ were used for the following analysis.

3. Structure refinements

All least-squares refinements reported below were carried out with the program *MOLLY* (Hansen & Coppens, 1978). The atomic scattering factors for the free atoms were calculated directly by the program from atomic

Table 1. *Experimental details*

Crystal data	
Chemical formula	B_3LiO_5
Chemical formula weight	119.37
Cell setting	Orthorhombic
Space group	$Pna2_1$
a (Å)	8.444 (2)
b (Å)	7.378 (2)
c (Å)	5.1416 (6)
V (Å^3)	320.3
Z	4
D_x (Mg m^{-3})	2.476
Radiation type	Ag $K\alpha$
Wavelength (Å)	0.56087
No. of reflections for cell parameters	20
θ range (°)	16–24
Limits of θ (°); sin θ/λ (Å^{-1})	0.5–35; 0–1.02
μ (mm^{-1})	0.1272
Temperature (K)	293 ± 2
Crystal form	Roughly isometric
Crystal radius (cm)	Mean 0.015, μr = 0.0191
Crystal color	Colorless
Data collection	
Diffractometer	CAD-4
Data collection method	θ–2θ scans
Scan width	0.70 + 0.45tan θ
Detector aperture (mm)	3.5 + 2.5tan θ
Absorption correction	None
No. of measured reflections	5388
No. of independent reflections	1534
No. of observed reflections	1439
Criterion for observed reflections	$I > 3\sigma(I)$
R_{int}	0.03
θ_{max} (°)	35
Range of h, k, l	$-17 \rightarrow h \rightarrow 17$
	$0 \rightarrow k \rightarrow 15$
	$0 \rightarrow l \rightarrow 10$
No. of standard reflections	3
Frequency of standard reflections (min)	180
Refinement	
Refinement on	F
R	0.0147
wR	0.0193
S	1.106
No. of reflections used in refinement	1439
No. of parameters used	204
Weighting scheme	$w = 1/\sigma^2(F)$
$(\Delta/\sigma)_{max}$	Between 1 and 2
$\Delta\rho_{max}$ (e Å^{-3})	0.1
$\Delta\rho_{min}$ (e Å^{-3})	−0.1
Extinction method	Isotropic, type I, Lorentzian
Extinction coefficient	g = 3.9 (2) × 10^{-4}
Source of atomic scattering factors	Clementi & Roetti (1974)

orbitals (Clementi & Roetti, 1974). The anomalous scattering amplitudes were taken from the *International Tables for Crystallography* (Creagh & McAuley, 1992). Owing to the weak anomalous dispersion for Ag $K\alpha$ radiation ($\Delta f'$ = −0.0004, 0.0004, 0.0056, $\Delta f''$ = 0.0000, 0.0004, 0.0036, respectively, for Li, B and O), no statistically significant differences were calculated in the course of structure refinements for the Friedel pairs. Therefore, it was not possible to choose the correct polarity or to determine whether the crystal is monodomain or not. Consequently, reflections were averaged in the Laue group *mmm*, leading to a set of 1439 unique reflections with $I > 3\sigma(I)$ and an internal consistency factor p = 0.03, where (see Table 1)

$$\sigma^2(I) = \sigma_c^2(I) + p^2I^2;$$

σ_c is the standard deviation estimated from the counting.

3.1. *Conventional refinement*

Free-atom scattering factors were used during this step. The refined parameters were: atomic positions and anisotropic displacement parameters together with a scale factor. Secondary extinction was corrected for according to Becker & Coppens (1974; type I isotropic extinction assuming a Lorentzian mosaic distribution). The ponderation scheme was $w = 1/\sigma^2(F)$. The full-matrix least-squares refinement resulted in the following agreement indices

$$R(F) = 0.0223, \quad wR(F) = 0.0299, \quad S = 1.632.$$

Atomic fractional coordinates and anisotropic displacement parameters are reported in Table 2.† Interatomic distances and angles are shown in Table 3. It can be stressed that the final interatomic distances and angles following the multipole refinements are comparable, within ±1σ, to those of a high-angle refinement (sin θ/λ > 0.65 Å^{-1}), including only the scale factor, atomic coordinates and anisotropic thermal parameters. Fig. 1 shows a projection of the structure onto the *ab* plane and an *ORTEP* view (Johnson, 1965) of the B_3O_7 cluster.

3.2. *Description of the structure*

The crystal structure is built up of a three-dimensional network of B_3O_7 groups composed of two B(1) atoms linked to O(1), O(2) and O(3), and B(2) linked to O(2), O(4) and O(5), as well as B(3) linked tetrahedrally to O(1), O(3), O(4) and O(5). The sequence B(1), O(2), B(2), O(5), B(3), O(3) forms a hexagonal ring and these atoms are at most 0.06 Å out of the calculated mean-squares plane. This picture will be used frequently to describe the deformation density (mean plane B_3O_3). However, in fact, the angle between the two planes formed by O(1), O(2) and O(3) atoms around B(1), and O(2), O(4) and O(5) atoms around B(2) is 16.0 (4)°. The two BO_3 triangles are in a *syn* configuration with respect to the plane defined by O(2), O(3), O(5) and B(3). This true geometry will always be used in the detailed description of the deformation density.

In the BO_4 tetrahedron, the four B—O bonds are divided into two statistically different groups: B(3)—

† Tables corresponding to atomic coordinates, displacement parameters, interatomic distances and angles are those obtained at the end of the multipole refinements. Intermediate parameters are not mentioned.

Table 2. *Fractional atomic coordinates and anisotropic displacement parameters ($Å^2$)*

	x	y	z	U^{11}	U^{22}	U^{33}	U^{12}	U^{13}	U^{23}
Li	−0.08716 (18)	0.56672 (15)	1.04979 (30)	0.02373 (49)	0.01044 (34)	0.02259 (54)	0.00155 (32)	−0.00682 (38)	−0.00300 (36)
B(1)	−0.00966 (5)	0.16429 (6)	0.90497 (11)	0.00846 (12)	0.00605 (12)	0.00651 (12)	−0.00026 (9)	0.00172 (10)	−0.00039 (10)
B(2)	−0.15710 (5)	0.24848 (5)	1.28469 (10)	0.00711 (11)	0.00500 (10)	0.00659 (12)	−0.0028 (9)	0.00102 (10)	−0.00144 (10)
B(3)	−0.19427 (5)	−0.05677 (6)	1.10169 (10)	0.00669 (11)	0.00522 (11)	0.00579 (12)	−0.00029 (9)	−0.00045 (10)	−0.00101 (10)
O(1)	0.11613 (4)	0.20462 (4)	0.74900	0.00837 (9)	0.00570 (8)	0.00867 (10)	0.00018 (7)	0.00348 (7)	−0.00003 (8)
O(2)	−0.05807 (4)	0.29785 (4)	1.08035 (9)	0.01047 (10)	0.00599 (10)	0.00812 (10)	−0.00108 (7)	0.00403 (8)	−0.00133 (8)
O(3)	−0.08649 (4)	0.00438 (4)	0.89782 (9)	0.01072 (9)	0.00696 (8)	0.00754 (9)	−0.00219 (7)	0.00336 (8)	−0.00202(8)
O(4)	−0.16126 (4)	0.37480 (4)	1.47909 (9)	0.00671 (8)	0.00712 (9)	0.00909 (10)	−0.00051 (7)	0.00210 (8)	−0.00426 (8)
O(5)	−0.23880 (4)	0.09032 (4)	1.28520 (9)	0.00789 (9)	0.00532 (8)	0.00677 (9)	−0.00142 (7)	0.00155 (8)	−0.00222 (8)

O(3) and B(3)—O(4) close to 1.4614 (7) Å; B(3)—O(1) and B(3)—O(5) close to 1.4847 (7) Å. In the two triangles B(1)O(1)O(2)O(3) and B(2)O(2)O(4)O(5) there are also statistically different interatomic distances which can be grouped as follows

B(1)—O(2) and B(2)—O(2)
B(1)—O(3) and B(2)—O(5)
B(1)—O(1) and B(2)—O(4).

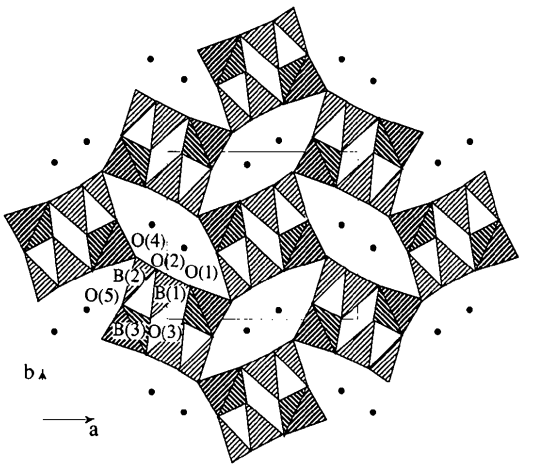

(*a*)

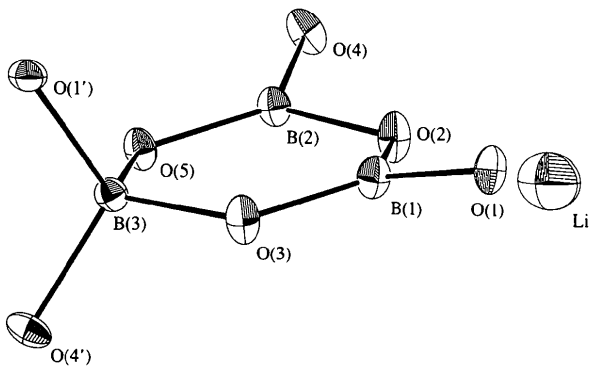

(*b*)

Fig. 1. (*a*) Projection of the structure along the **c** axis; (*b*) *ORTEP* view (Johnson, 1965) of the LiB_3O_7 cluster (probability level: 60%).

Table 3. *Selected interatomic distances (Å) and angles (°); B—O bonds in Table 5*

$B(1)O_3$ triangle			
O(1)—O(2)	2.3536 (6)	O(1)—B(1)—O(2)	116.97 (5)
O(1)—O(3)	2.3865 (4)	O(1)—B(1)—O(3)	123.38 (5)
O(2)—O(3)	2.3720 (5)	O(2)—B(1)—O(3)	119.64 (5)
$B(2)O_3$ triangle			
O(2)—O(4)	2.2988 (9)	O(2)—B(2)—O(4)	112.89 (5)
O(2)—O(5)	2.4048 (7)	O(2)—B(2)—O(5)	122.19 (6)
O(4)—O(5)	2.4141 (6)	O(4)—B(2)—O(5)	124.92 (6)
$B(3)O_4$ tetrahedron			
O(1)—O(3)	2.3876 (4)	O(1)—B(3)—O(3)	108.46 (4)
O(1)—O(4)	2.4089 (6)	O(1)—B(3)—O(4)	109.71 (4)
O(1)—O(5)	2.4172 (5)	O(1)—B(3)—O(5)	108.99 (5)
O(3)—O(4)	2.3719 (4)	O(3)—B(3)—O(4)	108.49 (6)
O(3)—O(5)	2.4542 (6)	O(3)—B(3)—O(5)	112.82 (4)
O(4)—O(5)	2.3912 (7)	O(4)—B(3)—O(5)	108.33 (4)
Lithium (all other distances are greater than 2.5 Å)			
Li—O(1)	1.9887 (18)	O(1)—Li—O(2)	144.48 (12)
Li—O(2)	2.0051 (17)	O(1)—Li—O(5)	100.67 (8)
Li—O(5)	2.0101 (21)	O(1)—Li—O(4)	92.09 (7)
Li—O(4)	2.1722 (19)	O(2)—Li—O(5)	103.20 (8)
		O(2)—Li—O(4)	95.24 (7)
		O(4)—Li—O(5)	125.13 (11)
Angles around the oxygen atoms in the B_3O_5 cluster			
B(1)—O(1)—B(3)	119.10 (4)		
B(1)—O(2)—B(2)	118.59 (5)		
B(1)—O(3)—B(3)	123.47 (4)		
B(2)—O(4)—B(3)	124.87 (5)		
B(2)—O(5)—B(3)	119.90 (5)		

The interatomic distances are statistically equal within each pair. Except for the B(3)—O(3) and B(3)—O(5) bonds (which are slightly different), closing the hexagon plane, the local symmetry of the B_3O_3 fragment is close to $\sigma_v(m)$. This observation will be used throughout the valence-electron density study.

4. Valence-electron density analysis

4.1. *Qualitative analysis of the B—O bonds*

Starting from the results of the conventional refinements, it is possible to describe qualitatively the nature of the chemical bond. As will be seen below, the Li atom may be considered a Li^+ ion and its valence electron is transferred to the tetrahedrally coordinated B(3) ion, allowing the formation of four bonds with σ character.

Then the two remaining B atoms form mixed σ, π bonds with the neighbouring atoms O(1), O(2) and O(3) for B(1), and O(2), O(4) and O(5) for B(2). By applying a simple resonance model using the Lewis scheme, the differences between interatomic distances B(1)—O and B(2)—O are easily explained. The π-bond indices thus obtained are as follows: B(1), O(1), O(3) and B(2), O(4), O(5) 3/8; B(1), O(2) and B(2), O(2) 2/8, in accordance with the experimental interatomic distances. The greater the π-bond indices, the shorter the interatomic distances. The π-bond index is zero for the four tetrahedral B(3)—O.

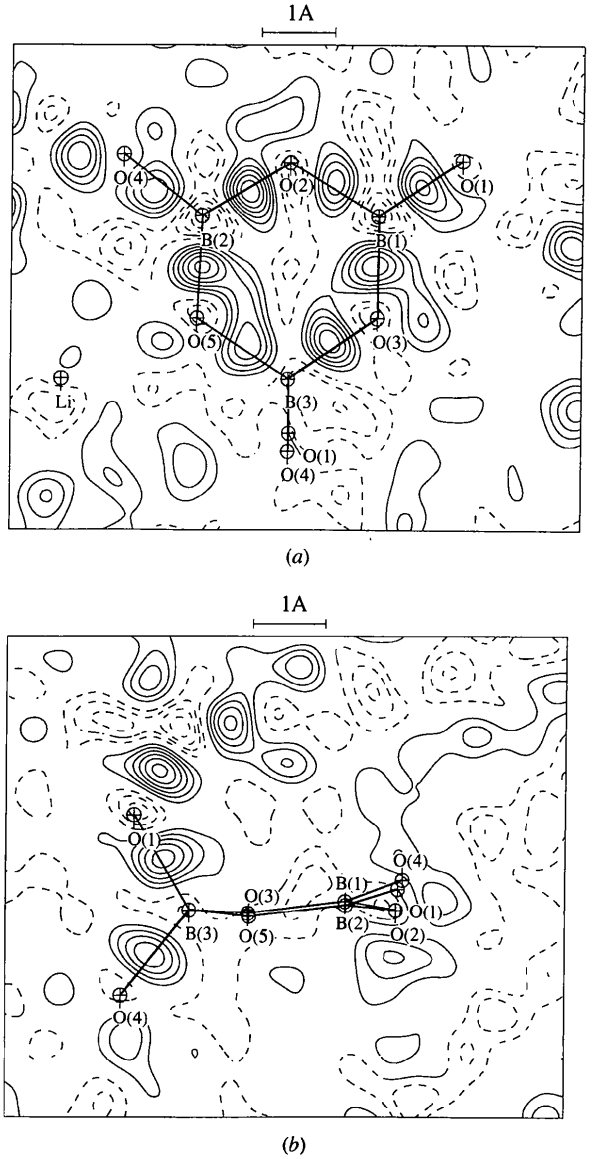

Fig. 2. Residual electron density map following free-atom refinement. (*a*) In the mean plane B_3O_3; (*b*) in the perpendicular plane through B(3) and O(2). Reflections with $\sin\theta/\lambda < 0.8$ Å^{-1}; all Fourier maps with contours at 0.05 e Å^{-3}; zero contour omitted.

Similar conclusions can be obtained using local molecular orbitals built up from atomic orbitals of B and O.

4.2. *Electron density refinements*

The residual Fourier maps (the phases of the independent atom model are attributed to the observed structure factors) calculated after the conventional refinements showed pronounced peaks between the B and O atoms (Fig. 2), as already discovered by Radaev *et al.* (1991, 1992).

Least-squares refinements were undertaken using the model of Hansen & Coppens (1978)

$$\rho_k(\mathbf{r}) = P_{k,\text{core}}\rho_{k,\text{core}}(r) + \left\{P_{k,\text{valence}}\kappa^3\rho_{k,\text{valence}}(\kappa r) + \sum_{l=1}^{4}\kappa'^3 R_{kl}(\kappa' r)\sum_{m=0}^{l}P_{klm}\pm Y_{klm}\pm(\theta_k,\varphi_K)\right\},$$

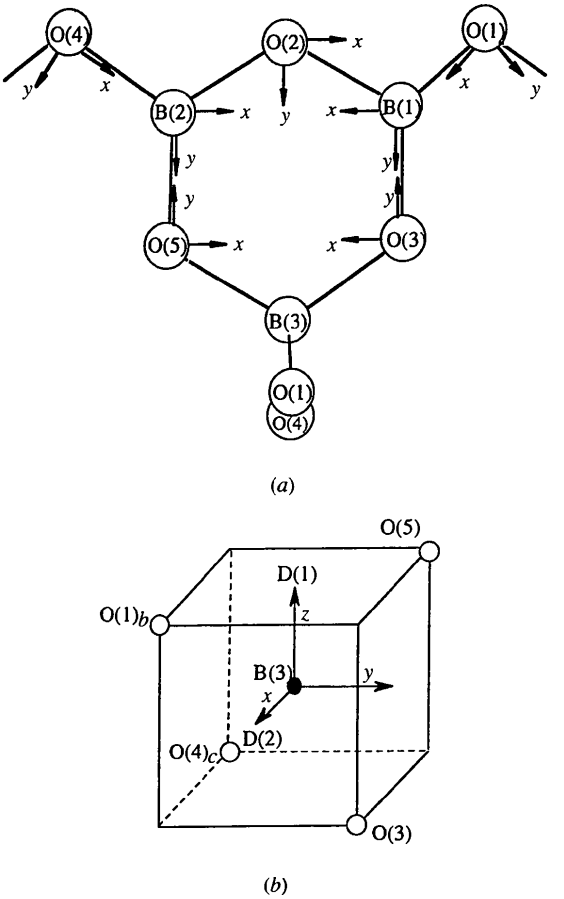

Fig. 3. Local Cartesian axes for the multipole functions in the asymmetric unit. (*a*) O and triangular B atoms; (*b*) tetrahedral B atom. D(1) and D(2) are at the centres of two adjacent faces of the cube.

where $\rho_{k,\text{core}}$ and $\rho_{k,\text{valence}}$ are spherically averaged Hartree–Fock core and valence densities, Y_{klm} are spherical harmonic angular functions in real form, $R_{kl}(\kappa' r)$ are Slater-type functions $r^{nl}\exp(-\zeta r)$, κ and κ' are the expansion–contraction parameters, and $P_{k,\text{valence}}$ and P_{klm} the population parameters. The n_l and ζ parameters used were, respectively: 2, 2, 3, 4, 6.00 Bohr^{-1} for oxygen and 2, 2, 3, 4, 3.00 Bohr^{-1} for boron. The local Cartesian axes used in the multipolar refinements are shown in Fig. 3.

4.3. *Kappa refinement*

The conventional free-atom model was first improved to account for the electronic charge transfer between atoms, keeping the unit-cell neutral. The atomic electron densities remain spherical. A parameter κ allows an isotropic expansion or contraction of the valence-electron density and the valence populations are varied (Coppens, Guru Row, Leung, Stevens, Becker & Yang, 1979). The five O atoms were constrained to have identical κ_O as were the three B atoms (κ_B).

In an early stage, the refinement showed that the valence population of lithium became strongly negative. We therefore imposed a zero valence population for this ion in the following cycles. The residual indices decreased to

$$R(F) = 0.0206, \quad wR(F) = 0.0284, \quad S = 1.508.$$

4.4. *Multipole refinements*

All atom coordinates are in positions corresponding to point symmetry 1. A multipolar refinement was undertaken with no restrictions on the multipolar function number and according to the local axes defined above. The κ and κ' parameters were constrained to be the same for the same element type and the charge of the Li atom was kept at +1. At convergence, the residual indices are remarkably low

$$R(F) = 0.0131, \quad wR(F) = 0.0183, \quad S = 1.083.$$

A residual electron density, calculated in the least-squares plane B_3O_3, does not show any contour greater than 0.05 e Å^{-3}. Unfortunately, as can be seen in Fig. 4, the deformation maps become physically meaningless.

This behaviour is discussed and explained elsewhere (El Haouzi, Hansen, Le Hénaff & Protas, 1995) and, briefly summarized, finds its origin in the fact that the space group is non-centrosymmetric. In that paper the case of LiB_3O_5 was discussed explicitly in detail.

To avoid the severe phase problem leading to some meaningless multipole function contributions, local non-crystallographic symmetry was introduced according to the structural results. Pseudo-symmetrically equivalent O(3) and O(5) as well as B(1) and B(2) atoms were constrained to have the same multipolar parameters (pseudo-mirror plane m) and O(2) to lie in the mirror. A pure tetrahedral symmetry was imposed on the B(3) atom which limits the multipoles to P_{32-}, P_{40} and P_{44+}, the latter being automatically determined to obtain the cubic harmonic function according to $x^4 + y^4 + z^4 - (3/5)\alpha(Y_{40} + 5Y_{44+})/20$ (see Hansen & Coppens, 1978). The local axes (Fig. 3) account for these constraints as well as charge transfers and multipole populations. The final multipole refinements, including atom coordinates, scale factor, anisotropic thermal parameters, extinction coefficient, valence populations, oxygen and boron κ as well as κ' and multipole parameters, yield

$$R(F) = 0.0147, \quad wR(F) = 0.0193, \quad S = 1.106.$$

16 reflections have an extinction correction y less than 0.8, and 5 less than 0.6 (111: 0.578; 201: 0.462; 211: 0.557; 221: 0.581; 401: 0.583).† An example of the corresponding dynamic and static maps in the mean plane B_3O_3 is shown in Figs. 5(*a*) and 5(*b*). Fig. 5(*a*) has been calculated to a higher resolution than the previous Fourier maps in order to facilitate comparison with the static maps (Fig. 5*b*) and also to show that the noise level in the experimental data is relatively low. Residual maps do not show any contour greater than ± 0.10 e Å^{-1}, close to the statistical error (0.05 e Å^{-1}) estimated from $\sigma^2(F)$ or $|F_{\text{obs}} - F_{\text{calc}}|^2$.

Dynamic experimental maps, dynamic model maps and residual maps were calculated using the program *JIMMY* (Hansen, 1996); static maps were calculated using the program *SALLY* (Hansen, 1996).

† Tables of valence and multipole populations, κ and κ' values, and lists of structure factors have been deposited with the IUCr (Reference: SH0093). Copies may be obtained through The Managing Editor, International Union of Crystallography, 5 Abbey Square, Chester CH1 2HU, England.

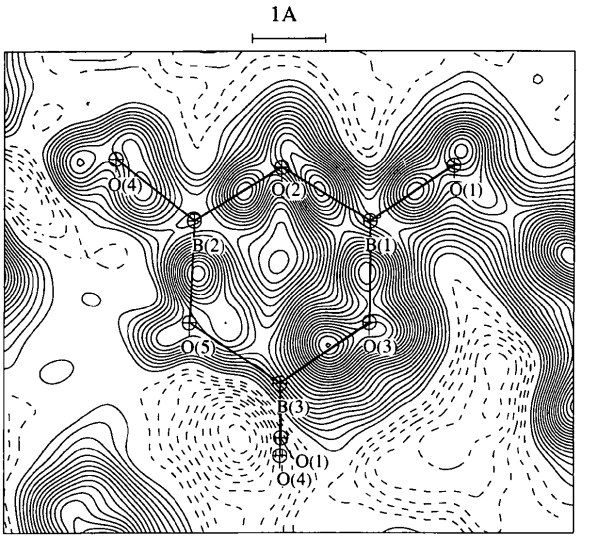

Fig. 4. Dynamic deformation density map in the mean plane B_3O_3 after the multipole refinement with no constraints. This map is clearly physically meaningless. Reflections with $\sin\theta/\lambda < 0.8$ Å^{-1}.

4.5. *Net charge calculations*

Fixing positional and thermal displacement parameters at the values obtained in the multipole refinement and keeping the Li charge fixed at +1, a refinement of κ and valence populations (Coppens *et al.*, 1979) was performed to obtain net charges on atoms (Table 4).

The calculated values show good agreement with what can be expected from the borate chemistry and clearly show the tendency of the triangular coordinated B(1) and B(2) atoms to acquire more electrons than the tetrahedrally coordinated B(3), explained by the σ–π covalency and the oxygen backdonation to the p_z orbital of these two atoms, as discussed below.

4.6. *Multipolar model analysis*

Peak heights in experimental, model and static deformation maps are shown in Table 5 with their corresponding distances to the B atoms. Figs. 6 and 7 show selected deformation maps around tetrahedral and triangular B atoms.

In the $B(3)O_4$ tetrahedron it can be seen, whatever the deformation map, that all maxima are almost equal and nearer oxygen than boron due to the greater electronegativity of oxygen. It can be noted that the B—O peak shapes (Fig. 6) are similar for the four bonds and display a cylindrical symmetry according to the σ-bond character.

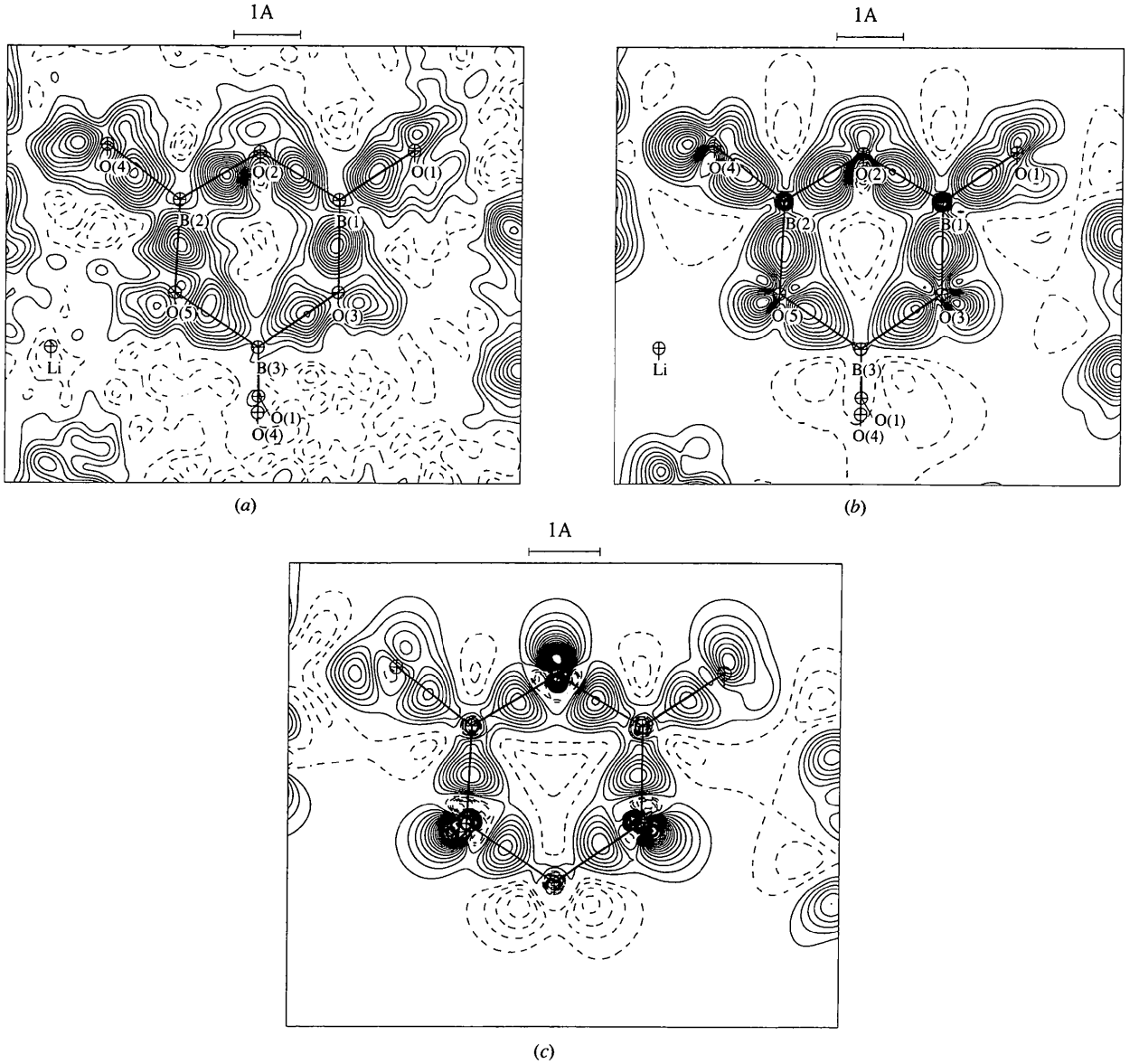

Fig. 5. Electron density deformation maps in the mean plane B_3O_3 (constrained multipole refinement, see text): (*a*) experimental dynamic map, all reflections; (*b*) static map; (*c*) calculated on a fragment $[B_9O_{19}H_8]^{3-}$ with a 6-31 g** basis set.

Table 4. *Experimental net charges (κ and P_v refinements; $R = 0.0217$, $wR = 0.0204$, $S = 1.56$, $N_{obs} = 1439$) and Mulliken net charges from a calculation with GAUSSIAN92 using a 6-31 g** basis set with a $[B_9O_{19}H_8]^{-3}$ fragment*

	κ(O) = 0.978 (3)				κ(B) = 1.087 (15)		
Atom	O(1)	O(2)	O(3),O(5)	O(4)	B(1),B(2)	B(3)	Li
Experimental	−0.59 (5)	−0.48 (6)	−0.52 (5)	−0.60 (5)	+0.52 (8)	+0.67 (8)	+1
Theory	−0.71	−0.63	−0.71,−0.68	−0.70	+0.74	+1.05	

Table 5. *B—O interatomic distances (Å), deformation density peak heights (e Å^{-3}) and distances B—M (Å) from the B atom to the deformation density maximum M (estimated error: $\Delta\rho \simeq 0.05$ e Å^{-3})*

Bond	B—O distance	Experimental		Model		Static		Theoretical	
		Height	B—*M*	Height	B—*M*	Height	B—*M*	Height	B—*M*
B(1)—O(1)	1.3638(7)	0.60	0.69	0.55	0.70	0.60	0.73	0.40	0.69
B(1)—O(2)	1.3969 (9)	0.60	0.79	0.50	0.83	0.60	0.89	0.45	0.74
B(1)—O(3)	1.3469 (6)	0.65	0.68	0.55	0.72	0.60	0.69	0.45	0.67
Mean		0.617		0.533		0.600		0.433	
B(2)—O(2)	1.3914 (9)	0.70	0.79	0.50	0.80	0.60	0.89	0.35	0.73
B(2)—O(4)	1.3671 (9)	0.50	0.74	0.50	0.70	0.55	0.67	0.40	0.70
B(2)—O(5)	1.3555 (7)	0.60	0.67	0.55	0.70	0.60	0.71	0.45	0.68
Mean		0.600		0.517		0.583		0.400	
B(3)—O(1)	1.4829 (7)	0.50	0.99	0.50	0.97	0.60	1.09	0.35	0.84
B(3)—O(3)	1.4597 (7)	0.50	0.90	0.40	0.93	0.50	1.02	0.30	0.84
B(3)—O(4)	1.4630 (8)	0.55	0.97	0.55	0.96	0.65	1.07	0.30	0.78
B(3)—O(5)	1.4864 (8)	0.45	0.96	0.45	0.96	0.50	1.04	0.35	0.85
Mean		0.500		0.475		0.562		0.325	

In $B(1)O_3$ and $B(2)O_3$ triangles the deformation peaks are broader in the plane perpendicular to the BO_3 plane (Fig. 7*c*) and correspond to the π-orbital electrons. Peak heights are still of the same order (Table 5) but, due to the π bonding, distances from the maximum to the neighbouring boron are now hardly different from half the interatomic distance.

4.7. *Lithium environment*

As shown in Table 3, lithium has four short interatomic Li—O distances (maximum: 2.1674 Å) with a distorted tetrahedral coordination. Deformation density maps demonstrate the choice of Li^+ to be appropriate (maps not shown). The lone pair regions of O(1), O(2), O(4) and O(5) are oriented towards Li. This behaviour agrees with results of other studies, for instance, $LiBO_2$ (Kirfel *et al.*, 1983).

4.8. *Theoretical calculations*

Ab initio calculations of the electron density were undertaken, using the program *GAUSSIAN*92 (Frisch *et al.*, 1992) applied to a molecular fragment $[B_9O_{19}H_8]^{3-}$. This fragment consists of the juxtaposition of three structural sub-fragments $[B_3O_7]^{5-}$ (Fig. 1*b*): (i) the atoms of the asymmetric unit (Table 2) augmented by O(1′) and O(4′); (ii) a symmetrically equivalent fragment by an *n*-glide plane bridged by the O(4) atom; (iii) a symmetrically equivalent fragment by a twofold screw axis bridged by the O(1) atom. On each terminal oxygen [not of O(2) type] is added a H atom at a distance of 0.98 Å in the direction of an outer-neighbouring boron. In this way, the atoms of the asymmetric unit are surrounded as in the crystal, except that we have omitted the Li atoms. The Mulliken net charges obtained from this calculation for the central B_3O_5 fragment are given in Table 4. Their values are more extreme than those obtained from the κ refinement, which may be explained by the very different

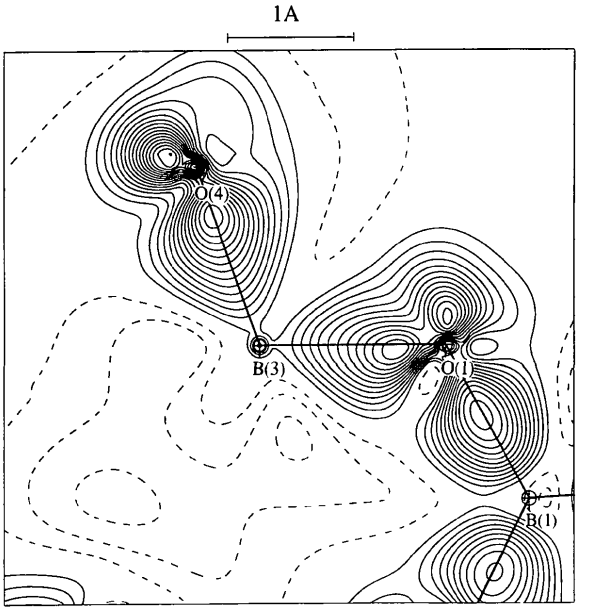

Fig. 6. Static electron density deformation map B(3)O(1)O(4) in the tetrahedrally coordinated B atom.

way in which the charges are defined for experiment and theory. Theoretical deformation density maps were calculated with the program *MODBG* (Hansen, 1996), which subtracts the total density of the spherical free atoms from the total density of the fragment. The best agreements were obtained using the 6-31g** basis set. An example of theoretical and static deformation density maps is reported in Figs. 5(*b*) and 5(*c*).

4.9. *Model of hybridized atoms*

The dynamic deformation density maps in planes perpendicular to the B_3O_3 ring (Fig. 7) show a clear lack of density, close to 0.15 e $Å^{-3}$, above and below B(1) and B(2), proving that the redistribution of electrons close to the atoms is quite different from spherical. These features are quite typical for B—O bonds, as seen for instance in the studies of $LiBO_2$ (Kirfel *et al.*, 1983, Fig. 5) or $Ca(BO_2)_2$ (Kirfel, 1987, Fig. 4). In order to obtain a clearer description of the effect of covalent bonding, we consider a deformation relative to hybridized atoms prepared for bonding in the same spirit as the work of Schwarz, Valtazanos & Ruedenberg (1985) and Kunze & Hall (1986). For the triangular B atoms, we assume a sp^2 hybridization with one electron in each of the lobes pointing towards the nearest neighbours and an empty p_z orbital. For oxygen, a pseudo-sp^2 hybridization according to the σ–π symmetries of the canonical molecular

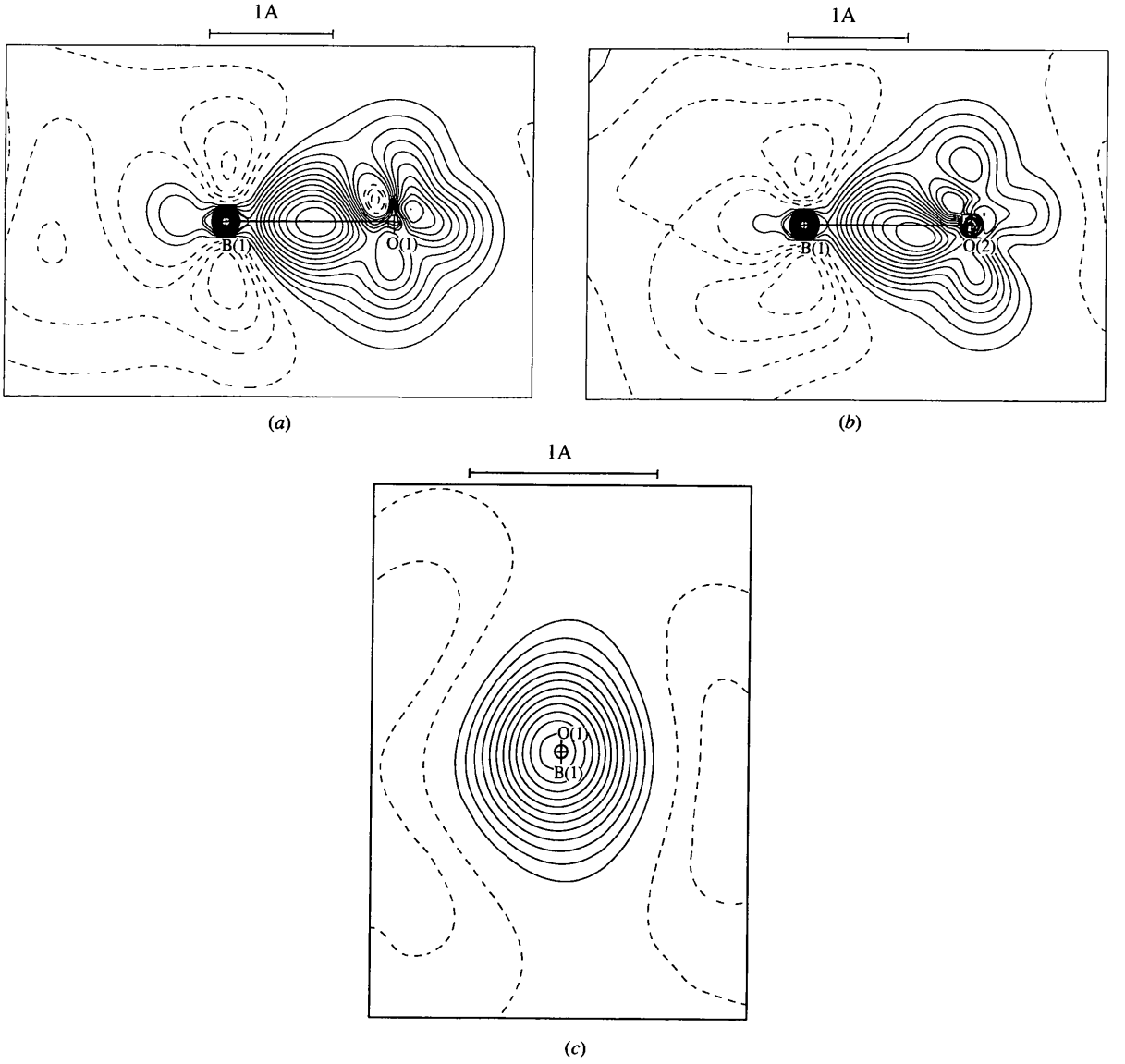

Fig. 7. Static electron density deformation maps in the triangularly coordinated B atom for (*a*) B(1)O(1), (*b*) B(1)O(2) and (*c*) in a plane perpendicular to the B—O bond at the maximum of the deformation density. The corresponding map for B(1)O(3) can be seen in Fig. 9.

orbitals may be assumed (it is noted that the B—O—B angles are close to 120°, see Table 3). The electron density of an O atom, placing one electron in either of the hybrids having lobes pointing towards neighbouring atoms and two electrons in the other two hybrid orbitals, is identical for sp^2 and sp^3 hybridization. We only have to impose that the angle between the lobes forming the σ bonds is equal to the bond angle. In Fig. 8 we show the difference in density between the hybridized atoms and the spherical ground state atoms, and we observe the same general features, though exagerated, as in the deformation maps (Fig. 7). Fig. 9(*b*) shows the static deformation density through a B—O bond when subtracting the hybridized instead of spherical atoms as in Fig. 9(*a*). Fig. 9 clearly illustrates the effect of bonding: an increase in density in the region of the p_z orbital of B and a decrease for the O atom. On the bond axis the density is strongly polarized towards the electronegative O atom and we may describe this situation as σ-donation–π-backdonation. The positive peaks behind the O atoms are due to the fact that O atoms are linked to other neighbouring borons. The apparent dissymmetry of the oxygen p_z orbital corresponds to a

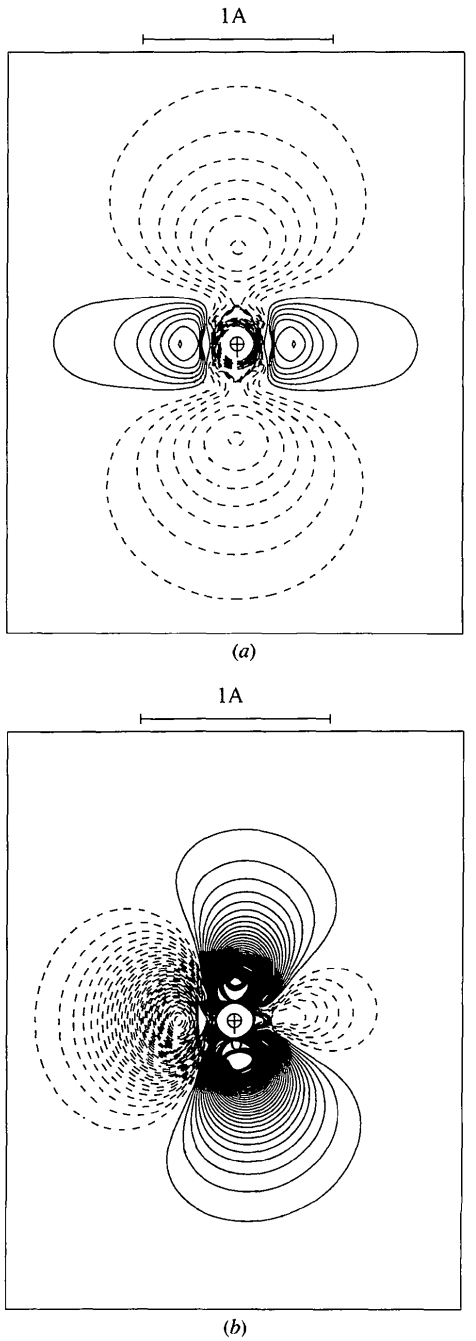

Fig. 8. Static difference density calculated by subtracting spherical from hybridized density. (*a*) In the spherical model of boron, a mean of 0.33 electrons is spread in the p_z orbital, whereas no electron is in this orbital in the sp^2-hybridized state. (*b*) In the spherical model of oxygen, 1.33 electrons are distributed in the p_z orbital, whereas 2 electrons are in this orbital in the sp^2-hybridized state. The bond axis is horizontal, pointing right for B, left for O; *z* axes are vertical.

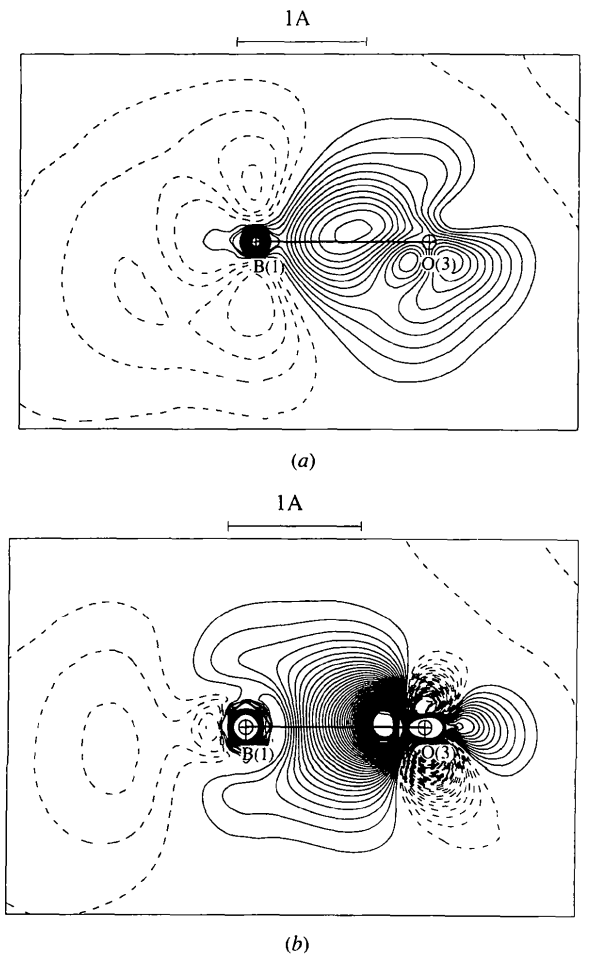

Fig. 9. Effect of a hybridized atom model on the static deformation map. For example, the B(1)—O(3) bond. (*a*) Spherical-atom model subtracted from the total static density. (*b*) Hybridized atom model subtracted from the total static density.

slight misorientation between neighbouring planes of B and O bonds. This is more pronounced for O(4).

These observations are confirmed when analysing the density matrix resulting from the Hartree–Fock calculation: the p_z orbital population of the triangularly coordinated B atom is 0.22 e^- and for the surrounding O atoms the p_z populations are 1.3, 1.4 and 1.5 e^- for O(1), O(2) and O(3), respectively.

5. Conclusions

This study shows good agreement between the experimentally and theoretically determined electron density distributions, in spite of severe phase problems for the non-centrosymmetric structure of LiB_3O_5. The major differences are in the description of the oxygen lone-pair electrons, a well known fact in other comparative studies of this type.

The experimental study clearly shows a π-electron transfer from the O atoms to the p_z orbitals of the triangular-coordinated B atoms. From the experiment we can only make a rough estimate of this transfer, of the order of a few tenths of an electron (less than 1/3, see caption Fig. 8), which is in agreement with values obtained from the theoretical density matrix.

Theoretical calculations were performed with the program package *GAUSSIAN*92 (Frisch *et al.*, 1992) in the 'Laboratoire de Chimie Théorique, Université Henri Poincaré-Nancy 1'. Dr Rinaldi and Dr Angyan are gratefully acknowledged for their help and fruitful discussions.

References

Becker, P. & Coppens, P. (1974). *Acta Cryst.* A**30**, 129–147.
Blessing, R. H. (1987). *Crystallogr. Rev.* **1**, 3–58.
Blessing, R. H. (1988). *Acta Cryst.* B**44**, 334–340.
Chen, C., Wu, Y., Jiang, A., Wu, B.,You, G., Li, R. & Lin, S. (1989). *J. Opt. Soc. Am.* **6**, 616–621.
Clementi, E. & Roetti, C. (1974). *At. Data Nucl. Data Tables*, **14**, 177–478.
Coppens, P., Guru Row, T. N., Leung, P., Stevens, E. D., Becker, P. J & Yang, Y. W. (1979). *Acta Cryst.* A**35**, 63–72.
Creagh, D. C. & McAuley, W. J. (1992). *International Tables for Crystallography*, Vol. C, Table 4.2.6.8. Dordrecht: Kluwer Academic Publishers.
El Haouzi, A., Hansen, N. K, Le Hénaff, C. & Protas, J. (1995). *Acta Cryst.* A**52**, 291–301.
Frisch, M. J., Trucks, G. W., Head-Gordon, M., Gill, P. M. W., Wong, M. W., Foresman, J. B., Johnson, B. G., Schegel, H. B., Robb, M. A., Replogle, E. S., Gomperts, R., Andres, J. L., Raghavachari, K., Binkley, J. S., Gonzalez, C., Martin, R. L., Fox, D. J., Defres, D. J., Baker, J., Stewart, J. J. P. & Pople, J. A. (1992) *GAUSSIAN*92. Revision A. Gaussian Inc., Pittsburg, PA.
Gajhede, M., Larsen, S. & Rettrup, S. (1986). *Acta Cryst.* B**42**, 545–552.
Hansen, N. K. (1996). *JIMMY, SALLY, MODBG.* Internal Programs. LCM3B. Université Henri-Poincaré Nancy 1, France.
Hansen, N. K. & Coppens, P. (1978). *Acta Cryst.* A**34**, 909–921.
Johnson, C. K. (1965). Report ORNL-3794. Oak Ridge National Laboratory, Tennessee, USA.
Kirfel, A. (1987). *Acta Cryst.* B**43**, 333–343.
Kirfel, A., Will, G. & Stewart, R. F. (1983). *Acta Cryst.* B**39**, 175–185.
Kunze, K. L. & Hall, M. B. (1986). *Am. Chem. Soc.* **108**, 5122–5127.
Le Henaff, C. (1996). Thesis. Université Henri-Poincaré-Nancy 1, France.
Marnier, G. (1986). Brevet, France. CNRS 2609976, 29 July 1986.
Marnier, G. (1988). United States Patent. CNRS 4746396, 24 May 1988.
Marnier, G., Boulanger, B. & Menaert, B. (1989). *J. Phys. Condens. Matter*, **1**, 4643–4648.
Radaev, S. F., Genkina, E. A., Lomonov, B. A., Maximov, B. A., Pisarevskii, Y. V., Chelokov, M. N. & Simonov, V. I. (1991). *Sov. Phys. Crystallogr.* **36**, 803–807.
Radaev, S. F., Maximov, B. A., Simonov, V. I., Andreev, B. V. & D'yakov, V. A. (1992). *Acta Cryst.* B**48**, 154–160.
Radaev, S. F., Muradyan, L. A., Malakhova, L. F., Burak, Y. V. & Simonov, V. I. (1989). *Sov. Phys. Crystallogr.* **34**, 842–846.
Sastry, B. S. R. & Hummel, F. A. (1958). *J. Am. Ceram. Soc.* **41**, 7–17.
Schwarz, W. H. E., Valtazanos, P. & Ruedenberg, K. (1985). *Theor. Chim. Acta*, **68**, 471–506.
Sommer-Larsen, P., Kadziola, A. & Gajhede, M. (1990). *Acta Cryst.* A**46**, 343–351.